

Antibunching and bunching of photons in resonance fluorescence from a few atoms into guided modes of an optical nanofiber

K. P. Nayak,¹ Fam Le Kien,¹ M. Morinaga,² and K. Hakuta¹

¹*Department of Applied Physics and Chemistry, University of Electro-Communications, Chofu, Tokyo 182-8585, Japan*

²*Institute for Laser Science, University of Electro-Communications, Chofu, Tokyo 182-8585, Japan*

(Received 17 June 2008; published 11 February 2009)

We experimentally investigate the photon correlations in resonance fluorescence from a few atoms into the guided modes of the nanofiber. We show that, when the photons are emitted in the same direction, the photon correlation varies from antibunching to bunching with increasing atom number and, when the photons are emitted in the opposite directions, the photon correlation is always antibunchinglike regardless of the number of atoms. The effect of excitation geometry on the photon correlations is also discussed.

DOI: [10.1103/PhysRevA.79.021801](https://doi.org/10.1103/PhysRevA.79.021801)

PACS number(s): 42.50.Ar, 42.50.Ct

The measurement of second-order (intensity) correlation of light using the Hanbury Brown–Twiss (HBT) interferometer is widely used in various fields of physics. The second-order correlation for the radiation from a multiemitter source can be described by the interplay between the first- and second-order coherences for a single emitter [1]. In fact, the original idea of a HBT interferometer was to extract information about the first-order coherence from the intensity correlation of light from a star containing a huge number of emitters [2]. Intensity correlations from a small number of emitters exhibit *photon antibunching* and have been investigated to explore the quantum nature of atoms and photons [3,4]. Such photon correlations in the resonance fluorescence of atoms have been systematically investigated by varying the atom number from one to a few atoms [5,6]. However, in such few-atom experiments the fluorescence is collected from a large solid angle and the first-order coherence is washed out due to the averaging over a continuum of spatial modes. In order to observe the interplay between the first- and second-order coherences, a key issue is to measure the correlations under the single-mode (small-solid-angle) condition. Grangier *et al.* [7] have measured the photon correlations in multiatom fluorescence under the single-mode condition. But since their measurements were done for a very large number of atoms, on the order of 10^6 , first-order coherence completely dominated the correlations and, hence, second-order coherence could not be observed. Depending on the observation geometry, they have observed two types of first-order coherences: bunching in the case of same-direction observation and antibunching in the case of opposite-direction observation. Photon correlations in both regimes—multimode observation of few-atom fluorescence and single-mode observation of multiatom fluorescence—have been investigated by Narducci [8]. However, an experimental demonstration of the interplay between the first- and second-order coherences in resonance fluorescence requires proper methods to efficiently observe the fluorescence photons from a few atoms under the single-spatial-mode condition. Hennrich *et al.* [9] have demonstrated the transition from antibunching to bunching in the photon correlations measured for an ensemble of cold atoms coupled to a single mode of a high-finesse optical cavity.

In the present work, we experimentally investigate the correlations between photons emitted from a few atoms us-

ing optical nanofibers. Since atoms around the nanofiber can emit photons efficiently into the guided modes of the nanofiber, one could efficiently detect the fluorescence photons from a few atoms in the single-mode regime at the ends of the fiber [10–12]. We demonstrate that when the photons are emitted in the same direction (one-end correlation), the photon correlation varies from antibunching to bunching with increasing atom number and, when the photons are emitted in the opposite directions (opposite-end correlation), the photon correlation is always antibunchinglike regardless of the number of atoms. We also demonstrate that the excitation geometry can be crucial to observe the antibunched-type first-order coherence in opposite-end correlations. The results suggest that the optical nanofiber method may be implemented as a promising tool for various quantum optics experiments. Apart from the fundamental interest, the present work can be of importance for establishing a concrete basis for all-fiber-based quantum communications coupled with cold-atom technologies.

First, we briefly describe the theoretical outline of the present multiatom emitter system. Atoms are distributed randomly around the nanofiber and emit photons into the guided modes. The field emitted by the atoms can be written as a sum of the fields emitted by individual atoms, and the second-order correlation function will contain various cross terms up to fourth power of the field amplitude. However, due to averaging over a random distribution of atom positions, most of the terms are averaged out to zero and the only persisting terms are due to the contributions from single and paired atoms. Details of the theory can be found in Ref. [13]. Following this formalism, the second-order correlation function can be written as

$$G_n^{(2)}(\tau) \propto n g^{(2)}(\tau) + n^2 \{ \mu_0 + \mu |g^{(1)}(\tau)|^2 \delta_{f_a, f_b} + \mu' |g^{(1')}(\tau)|^2 \delta_{f_a, -f_b} \}, \quad (1)$$

where n is the average atom number, f_a and f_b denote the observation directions, and τ denotes the delay time. In deriving the above formula, we have assumed the Poissonian distribution [1,4] for the atom number in the observation region. $g^{(2)}(\tau) \propto \langle A_j^\dagger(a) A_j^\dagger(b) A_j(b) A_j(a) \rangle$ is the second-order correlation function for emission from a single atom, while $g^{(1)}(\tau) \propto \langle A_j^\dagger(a) A_j(b) \rangle$ and $g^{(1')}(\tau) \propto \langle A_j^\dagger(a) A_j^\dagger(b) \rangle$ are the first-

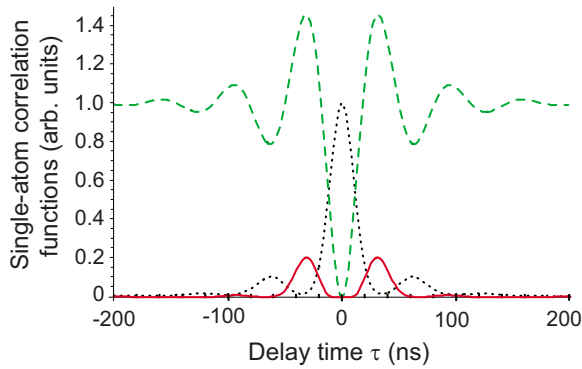


FIG. 1. (Color online) Single-atom correlation functions $g^{(2)}(\tau)$ (dashed curve), $|g^{(1)}(\tau)|^2$ (dotted curve), and $|g^{(1')}(\tau)|^2$ (solid curve) versus the delay time τ , calculated for the spontaneous emission time $\tau_{sp}=30$ ns and the Rabi frequency $\Omega=3/\tau_{sp}$.

order correlation functions. Here a and b denote the detector positions and A_j is the operator for the amplitude of the flux of photons emitted from the j th atom into the guided modes. The $g^{(2)}(\tau)$ term is due to the contribution from individual single atoms and scales as n in the correlation function $G_n^{(2)}(\tau)$, while the other terms are due to the contribution from paired atoms and scales as n^2 . Note that the $g^{(1)}(\tau)$ term contributes only to same-direction (one-end) correlations, while the $g^{(1')}(\tau)$ term contributes only to opposite-direction (opposite-end) correlations. It is due to the cancellation of the position-dependent phase factor $A_j(a) \propto e^{-if_a\beta_0 z_j}$, where β_0 denotes the longitudinal propagation constant for the guided mode and z_j is the position of the atom along the fiber axis [13]. The correlation function differs from that for free-space observation through the coefficients μ_0 , μ , and μ' , which are determined by the mode profile function of the guided modes. After averaging over the random position of atoms, the final expressions for the coefficients μ_0 , μ , and μ' depend on the dipole-moment orientation of atoms, the polarization of guided modes, and the transverse spread of the observation volume around the nanofiber.

To get insight into the behavior of the single-atom correlation functions, we plot them in Fig. 1. $g^{(2)}(\tau)$ and $|g^{(1)}(\tau)|^2$ show well-known antibunching and bunching behavior at zero delay, respectively. Meanwhile, $|g^{(1')}(\tau)|^2$ shows an antibunchinglike behavior at zero delay with wings at the delay times around the spontaneous emission time τ_{sp} . This behavior may naturally be understood from the fact that $g^{(1')}(\tau) \propto \langle A_j^\dagger(a)A_j^\dagger(b) \rangle$ describes the process in which one atom must emit two photons successively. Such two events can occur only with a finite delay around τ_{sp} . The photon correlations are dominated by the first-order coherences with increasing atom number, since the $g^{(1)}(\tau)$ and $g^{(1')}(\tau)$ terms scale as n^2 in the correlation function $G_n^{(2)}(\tau)$.

Figure 2 shows the conceptual diagram for the experiments. Experiments are performed by overlapping cold cesium atoms with an optical nanofiber and detecting the fluorescence photons emitted into the guided modes of the nanofiber [11,12]. The nanofiber is located at the waist of a tapered optical fiber which is produced by heating and pulling a commercial single-mode optical fiber. The diameter of the nanofiber is 400 nm, and the length is 2 mm. The length

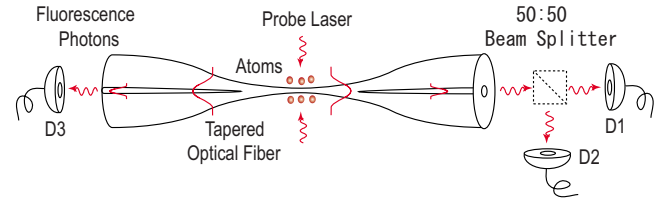


FIG. 2. (Color online) Conceptual diagram of the experiment. The nanofiber is located at the waist of a tapered optical fiber. Fluorescence photons emitted to the guided modes of the nanofiber are detected at the ends of the single-mode optical fiber using avalanche photodiodes ($D1$, $D2$, and $D3$).

of the single-mode fiber is 10 m on either side of the nanofiber. Cold cesium atoms are produced by using a magneto-optical trap (MOT) equipped with a resistively heated alkali-metal dispenser source. The MOT laser beams are switched off for 10 μ s periodically at an interval of 200 μ s. During the switched-off periods, atoms around the nanofiber are excited by a probe laser beam irradiated perpendicularly to the nanofiber. The probe laser is line-focused perpendicularly to the fiber axis, down to 100 μ m to spatially restrict the observation region. Two irradiation schemes are employed. One is to irradiate the probe beam to the nanofiber simply from one side (traveling-wave scheme), and the other is to reflect back the incident probe beam onto the nanofiber (standing-wave scheme). The polarization of the probe laser is perpendicular to the fiber axis. Atoms around the nanofiber emit an appreciable fraction of fluorescence photons into either direction-guided modes with equal probabilities [10,11]. Fluorescence photons are detected at the ends of the single-mode fiber using avalanche photodiodes (APDs, Perkin Elmer SPCM-AQR/FC). In the measurements, the dispenser current is adjusted to control the atom number in the observation region.

Photon correlations are measured using the HBT setup at one end and at opposite ends of the nanofiber for both traveling-wave and standing-wave irradiation schemes. For the one-end observation scheme, the fluorescence light at one end of the fiber is split into two using a 50:50 nonpolarizing beam splitter, and the photons are detected by the APDs $D1$ and $D2$. Meanwhile, for the opposite-end observation scheme, the beam splitter is removed and the photons are detected by the APDs $D1$ and $D3$. The correlations are measured using a time-correlated photon counter (TimeHarp-200, PicoQuant GmbH) in the single-stop mode with time resolution of 1 ns for delay time up to ± 100 ns.

Figures 3(a) and 3(b) exhibit the measured correlations for the traveling-wave scheme for the one-end and opposite-end measurements, respectively, for three different dispenser currents. In these measurements, the probe laser frequency is tuned close to the resonance with atomic transition $6S_{1/2} F=4 \leftrightarrow 6P_{3/2} F'=5$. The measured probe beam intensity, averaged over the observation region, is $I_{avg} \sim 30$ mW/cm². The number of photons scattered from the nanofiber is at least one order smaller than that of the fluorescence photons and gives a negligible contribution to the measured correlations. For the lowest dispenser current, $I_D=3.8$ A, the results for both types of observation schemes show clearly antibunching of fluorescence photons at zero delay as well as Rabi oscil-

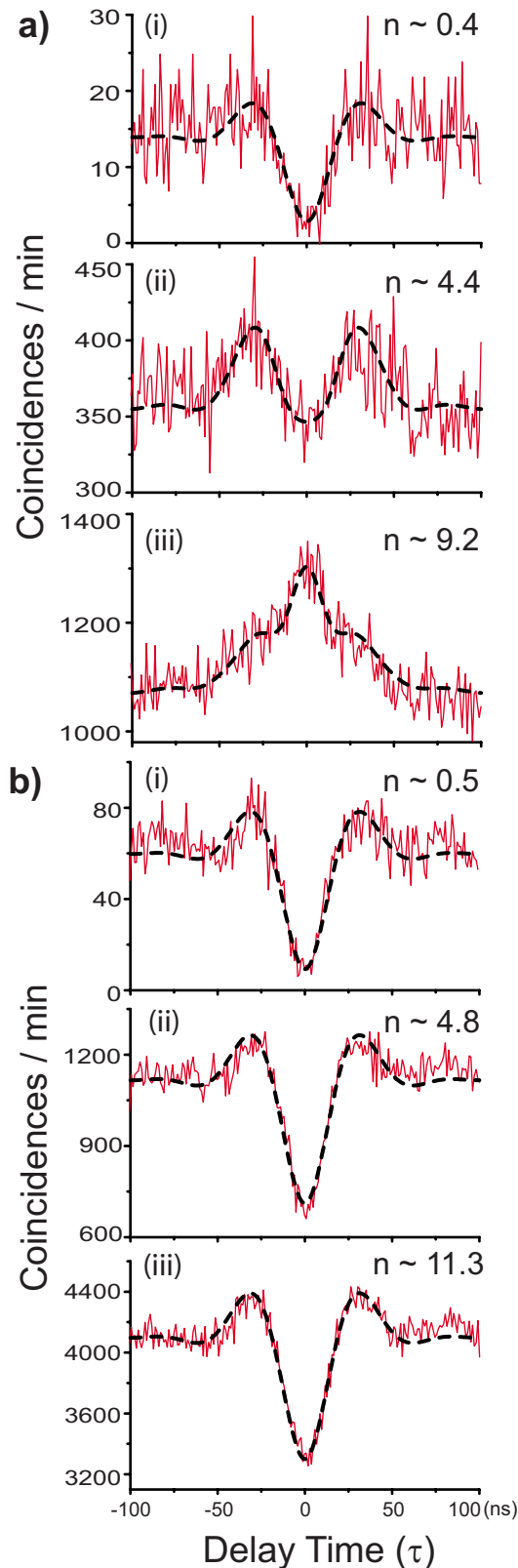


FIG. 3. (Color online) Second-order correlations (solid curves) between photons emitted into the nanofiber, measured in the (a) one-end and (b) opposite-end observation schemes for three different dispenser currents (i) 3.8 A, (ii) 4.6 A, and (iii) 5.0 A. In these measurements, the excitation field was a traveling wave. For comparison, we show the theoretical fittings (dashed curves) and the estimated average atom numbers n .

lations in the wings. But for higher dispenser currents there is a drastic difference between the two types of correlations. For the one-end correlation, the antibunching dip is suppressed with increasing the dispenser current and finally shows a bunching behavior for $I_D=5.0$ A. Meanwhile, for the opposite-end correlation, the antibunching behavior persists for higher dispenser currents.

The experimental results shown in Figs. 3(a) and 3(b) are fitted using Eq. (1). Since the probe beam is line-focused, its intensity profile in the observation region is not uniform. In order to take into account this fact, we perform averaging over the intensity distribution assuming a Gaussian profile along the fiber axis with a peak value of 50 mW/cm^2 and a $1/e^2$ -diameter of $100 \mu\text{m}$. For the fittings we use $\tau_{sp}=30 \text{ ns}$, while the average atom number n and the coefficients μ_0 , μ , and μ' are the adjusting parameters. For the one-end correlations, the fittings have led to the average atom numbers $n \sim 0.4$, 4.4 , and 9.2 for dispenser currents $I_D=3.8$ A, 4.6 A, and 5.0 A, respectively, with the coefficients $\mu_0=0.36$ and $\mu=0.22$.¹ The fittings reproduce the experimental results quite well, revealing that the correlations vary from antibunching to bunching with increasing atom number due to the interplay between the second-order $g^{(2)}(\tau)$ and first-order $g^{(1)}(\tau)$ terms. However, the experimental results for the opposite-end correlations could not be reproduced by using the above obtained coefficients. If we assume $\mu'=0.22$, for the dispenser current $I_D=5.0$ A, the wings at around $\tau \sim 30 \text{ ns}$ will be almost twice larger than the observation. The observations are better reproduced using $\mu'=0$ —that is, without the effect of the $g^{(1)}(\tau)$ term. The fittings for the three dispenser currents have led to average atom numbers of $n \sim 0.5$, 4.8 , and 11.3 , revealing good correspondence to the atom numbers estimated for the one-end correlation [see Fig. 3(a)]. We must mention that the photon correlations in the longer time scale show a decay behavior at a time constant of $1.8 \mu\text{s}$ as discussed in Ref. [12], revealing the dwell time of single atoms in the observation region.

Next, we discuss the correlations measured in the standing-wave irradiation scheme. Regarding the one-end correlations, both types of irradiation schemes give similar results. However, for the opposite-end correlations, a significant difference has been observed for high dispenser currents. The measured opposite-end correlations at a dispenser current $I_D=5.2$ A for the standing-wave and traveling-wave schemes are plotted in Figs. 4(a) and 4(b), respectively. In these measurements the excitation intensity is kept the same for both the schemes with $I_{avg} \sim 60 \text{ mW/cm}^2$ and the probe laser frequency is detuned 16 MHz below the atomic resonance. One can easily see that the wings are higher for the standing-wave scheme than for the traveling-wave scheme. The observation suggests that, for the opposite-end observation scheme, the first-order $g^{(1)}(\tau)$ term can affect the pho-

¹Assuming an observation region of 500 nm thickness around the nanofiber and after averaging over the polarizations of guided modes, the coefficients μ_0 and μ are theoretically estimated to be in the range $0.33\text{--}0.37$ and $0.17\text{--}0.35$, respectively, depending on the dipole-moment orientations of the atoms. μ and μ' take the same value after averaging over the polarizations of the guided modes.

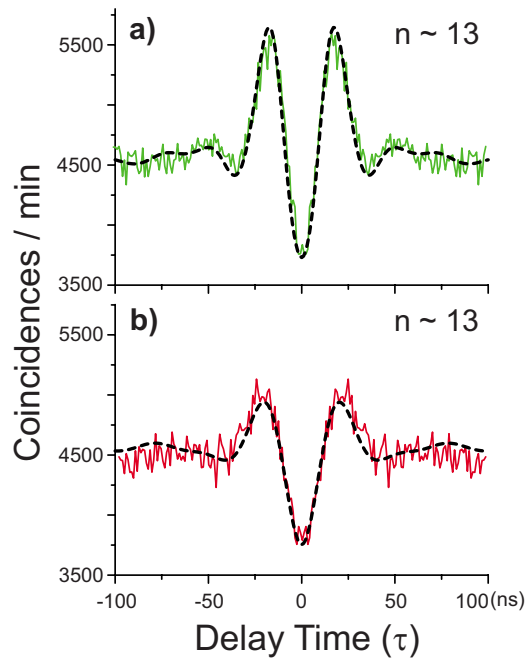


FIG. 4. (Color online) The measured opposite-end correlations (solid curves) for two excitation schemes: (a) standing wave and (b) traveling wave. Dashed curves are the theoretical fittings. $n \sim 13$ denotes the estimated average atom number.

ton correlations when the excitation field is a standing wave.

Such a dependence of the opposite-end correlations on the excitation geometry may be understood as an effect of the spatial dependence of the phase of the excitation beam and the transverse spread of the atom-position distribution in the observation region around the nanofiber. As already mentioned, the single-atom correlation function $g^{(1)}(\tau)$ describes two successive emission events and, hence, the corresponding excitation process is two successive excitation events which can be effectively expressed by the square of the negative frequency component of the incident field amplitude: namely, $[E^{(-)}(\mathbf{r}_j)]^2$. The spatial dependence of the frequency component $E^{(-)}(\mathbf{r}_j)$ can be expressed as $E^{(-)}(\mathbf{r}_j) \propto e^{-i\mathbf{k}\cdot\mathbf{r}_j} + \alpha e^{i\mathbf{k}\cdot\mathbf{r}_j}$, where \mathbf{k} is the wave vector of the forward propagating beam, \mathbf{r}_j denotes the atom position, and α is the relative amplitude of the reflected beam. Hence, we have $g^{(1)}(\tau) \propto (e^{-i\mathbf{k}\cdot\mathbf{r}_j} + \alpha e^{i\mathbf{k}\cdot\mathbf{r}_j})^2$. For the standing-wave excitation scheme, we have $\alpha \sim 1$ and, therefore, the $g^{(1)}(\tau)$ term will appear in the correlation function through the cross

terms in $(e^{-i\mathbf{k}\cdot\mathbf{r}_j} + \alpha e^{i\mathbf{k}\cdot\mathbf{r}_j})^2$, which are independent of the atom position. Meanwhile, for the traveling-wave excitation scheme we have $\alpha=0$. In this case, the $g^{(1)}(\tau)$ term will be negligible due to the averaging over the transverse spread of the atom position if the spread is larger than half the wavelength of the excitation beam. In the present experiments, the observation region can be considered as a cylindrical volume around the nanofiber with a thickness of 500 nm [10,11] and the size of the transverse spread can be estimated to be $\sim 1.4 \mu\text{m}$, which is larger than the excitation field wavelength $\lambda \sim 850 \text{ nm}$. Note that the above excitation-geometry effect does not appear in both the $g^{(2)}(\tau)$ and $g^{(1)}(\tau)$ terms, since the field operators appear as conjugate pairs.

The experimental results are fitted following similar procedure as discussed for Fig. 3. The coefficients used for the fittings are $\mu'=0.22$ for the standing-wave scheme ($\alpha=1$) and $\mu'=0$ for the traveling-wave scheme ($\alpha=0$) and $\mu_0=0.36$ for both the schemes. The estimated average atom number is $n \sim 13$ for both fittings. The fitted results are in good agreement with the experimental results, revealing that the excitation geometry plays a crucial role for observing the $g^{(1)}(\tau)$ term in the opposite-end correlation. This can explain the observations in Fig. 3(b) with $\mu'=0$. This kind of geometrical effect was pointed out by Grangier *et al.* [7] in the case of atoms in free space. They attributed its origin to a phase-matching condition due to some spontaneous four-wave-mixing process. The present understanding explains the results from a different viewpoint which could clarify the physics more naturally.

In summary, we have experimentally investigated the photon correlations in resonance fluorescence from a few atoms into guided modes of a nanofiber. We have demonstrated that the correlation between photons emitted in the same direction varies from antibunching to bunching with increasing atom number, while that for photons emitted in the opposite directions is always antibunchinglike regardless of the number of atoms. We have shown that, unlike the same-direction observation scheme, the photon correlation observed in the opposite-direction scheme is substantially affected by the spatial dependence of the phase of the excitation field.

We are thankful to Manoj Das for technical assistance. This work was carried out under the 21st Century COE program on ‘‘Innovation in Coherent Optical Science.’’

- [1] R. Loudon, *Quantum Theory of Light*, 3rd ed. (Oxford University Press, Oxford, 2000).
- [2] R. Hanbury Brown and R. Q. Twiss, *Nature (London)* **178**, 1046 (1956).
- [3] H. J. Kimble, M. Dagenais, and L. Mandel, *Phys. Rev. Lett.* **39**, 691 (1977).
- [4] H. Paul, *Rev. Mod. Phys.* **54**, 1061 (1982).
- [5] F. Diedrich and H. Walther, *Phys. Rev. Lett.* **58**, 203 (1987).
- [6] V. Gomer, B. Ueberholz, S. Knappe, F. Strauch, D. Frese, and D. Meschede, *Appl. Phys. B: Lasers Opt.* **67**, 689 (1998).
- [7] P. Grangier, G. Roger, A. Aspect, A. Heidmann, and S.

Reynaud, *Phys. Rev. Lett.* **57**, 687 (1986).

- [8] F. A. Narducci, Ph.D. thesis, University of Rochester, 1996.
- [9] M. Hennrich, A. Kuhn, and G. Rempe, *Phys. Rev. Lett.* **94**, 053604 (2005).
- [10] F. Le Kien, S. Dutta Gupta, V. I. Balykin, and K. Hakuta, *Phys. Rev. A* **72**, 032509 (2005).
- [11] K. P. Nayak, P. N. Melentiev, M. Morinaga, F. L. Kien, V. I. Balykin, and K. Hakuta, *Opt. Express* **15**, 5431 (2007).
- [12] K. P. Nayak and K. Hakuta, *New J. Phys.* **10**, 053003 (2008).
- [13] F. Le Kien and K. Hakuta, *Phys. Rev. A* **77**, 033826 (2008).